Biochimica et Biophysica Acta 1808 (2011) 323–331

Contents lists available at ScienceDirect

Biochimica et Biophysica Acta

journal homepage: www.elsevier.com/locate/bbamem

Lipid chain branching at the iso- and anteiso-positions in complex chlamydia membranes: A molecular dynamics study

Joseph B. Lim, Jeffery B. Klauda *

Department of Chemical and Biomolecular Engineering, University of Maryland, College Park, MD 20742, USA

ARTICLE INFO

Article history:
Received 25 June 2010
Received in revised form 28 July 2010
Accepted 29 July 2010
Available online 6 August 2010

Keywords:
Chlamydia trachomatis
Lipid chain branching
Cholesterol
Complex membranes
Molecular dynamics

ABSTRACT

Membranes in the intracellular eubacterial parasite *Chlamydia trachomatis* consist of the elementary body (EB) and reticular body (RB), and contain methyl branches at the iso- and anteiso-positions for some phospholipid chains. Acyl chain branching is the focus of this study. Molecular dynamics simulations were used to study bilayers of 1-13-methylpentadecanoyl-2-palmitoyl-phosphatidylcholine (13-MpPPC), 1-14-methylpentadecanoyl-2-palmitoyl-phosphatidylcholine (14-MpPPC), and diphytanoylphosphatidylcholine (DPhPC). These three membranes were simulated at 323 K and simulations of DPhPC at 298 K were also performed for better comparison to existing experimental data. Two simulations of representative EB and RB membranes of *C. trachomatis* composed of nine different lipid components were performed at 310.15 K, to accurately reflect compositions determined by experiment and physiological conditions. Based on nearly 0.5 μs of simulation data, we report that branching increases average lipid surface area, area elastic moduli, and lipid axial relaxation times, while decreasing lipid chain order. Branching also has a distinct effect on electron density profiles. Due to their high cholesterol concentrations, the EB and RB membranes were found to have relatively high area elastic moduli, which may have important biological implications.

1. Introduction

The bacterium *Chlamydia trachomatis* is an obligate intracellular human pathogen that can give rise to genital and eye disease, as well as numerous reproductive problems. Chlamydia infection is one of the most common sexually transmitted infections worldwide, and can be especially problematic in developing countries due to the sophisticated equipment and training required for diagnosis and treatment. Certain peptides from the major outer membrane porin protein have been suggested to be a vaccine candidate that may be useful and cost-effective in developing regions [1,2]. Complete understanding of this protein and its fragments requires knowledge of its membrane environment and the biological processes underlying chlamydia infection.

Upon infection of the host cell, the bacterium is known to undergo a biphasic life cycle [3,4]. The elementary body (EB), a small, dormant cell type, initiates infection and enters the host cell. EBs differentiate into reticular bodies (RBs), which are larger, metabolically more active cell bodies. The RBs undergo replication in a chlamydial inclusion, which consists of a membrane-bound vacuole. After approximately 16 to 20 h, some RBs differentiate back into EBs while other RBs continue replication. This cycle repeats until approximately 2 to 3 days after infection, at which point the pathogens in the cell consist mainly of EBs. Lysis of the host cell releases the EBs to infect new host cells [3,4].

From a biophysical standpoint, the membranes of the EB and RB cell types are distinct from their eukaryotic hosts due to the presence of iso- and anteiso-branched chains in the phospholipids of the EB and RB. Although our work is on chlamydia membranes, chain branching is not unique to chlamydia and is common in many bacteria [5]. Previous experimental studies on chain branching have focused on diphytanoylphosphatidylcholine (DPhPC), a phospholipid with methyl branches at the 3, 7, 11, and 15 positions in both chains (Fig. 1) [6–8]. Molecular dynamics (MD) simulations have also been used to study DPhPC bilayers in atomic detail, revealing additional structural and dynamical properties not provided by experimental data, such as deuterium order parameters, diffusion constants, and electron density profiles [9–16].

However, there is a paucity of biophysical data available for iso- and anteiso-branched lipids. Furthermore, while experiments and simulations have been used to study DPhPC in great detail, the release of the CHARMM36 (C36) lipid force field presents an opportunity to study these branched lipids with a more accurate force field that can be simulated in the tensionless ensemble [17]. Hence, this study had several motivations. The first was to use the lipids 1-13-methylpentadecanoyl-2-palmitoyl-phosphatidylcholine (13-MpPPC), 1-14-methylpentadecanoyl-2-palmitoyl-phosphatidylcholine (14-MpPPC) and DPhPC (Fig. 1) to provide a comparison of branching effects on overall bilayer properties. The second was to investigate DPhPC using the updated C36 lipid force field and validate the branched chain

* Corresponding author. Tel.: +1 301 405 1320; fax: +1 301 314 9126.
E-mail address: jbklauda@umd.edu (J.B. Klauda).

0005-2736/$ – see front matter © 2010 Elsevier B.V. All rights reserved.
doi:10.1016/j.bbamem.2010.07.036

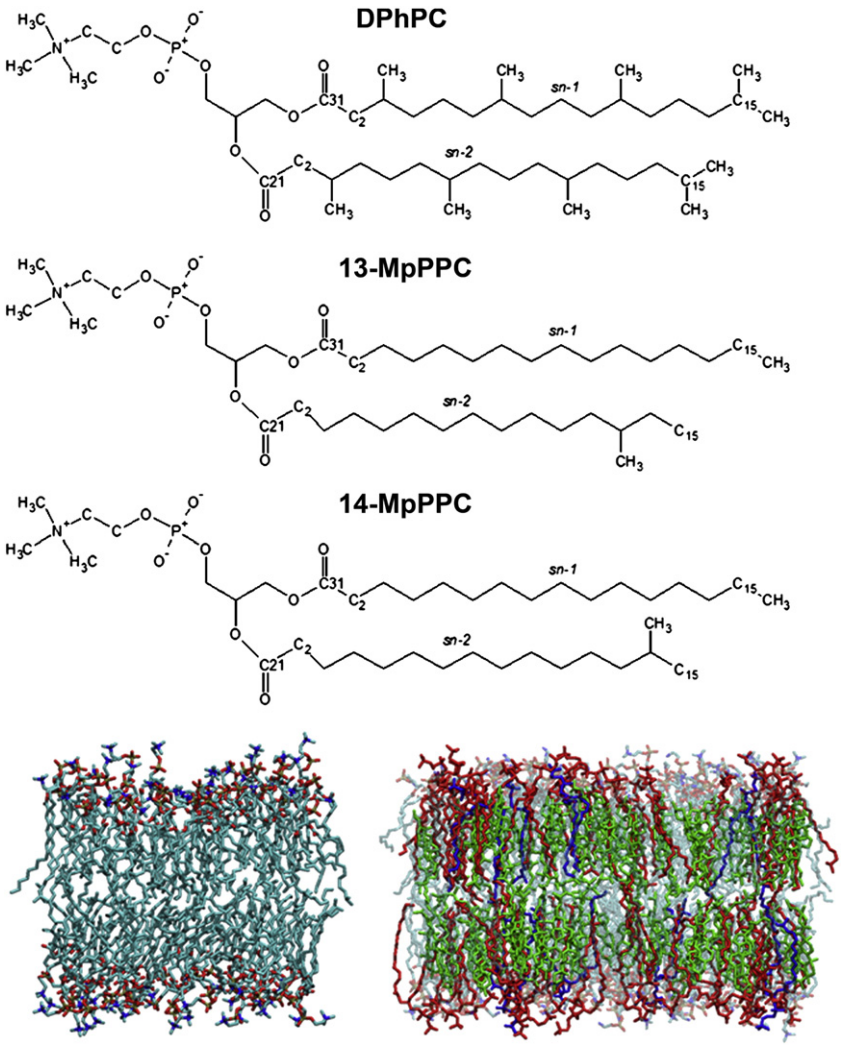

Fig. 1. Schematic drawings of DPhPC, 13-MpPPC, and 14-MpPPC. Final snapshots of 14-MpPPC (bottom left) and EB (13-MpPPC colored blue, 14-MpPPC colored red, cholesterol colored green, remaining lipids transparent).

topology. Lastly, 13-MpPPC and 14-MpPPC were simulated in complex membranes modeling the EB and RB membranes, to determine the effect of these lipids on membrane properties in physiological conditions, as well as the effect of the complex membrane environment on the behavior of branched chain lipids.

The EB and RB membranes in this study consisted of 9 different lipid types each. The lipid compositions of the EB and RB membranes found in experiment were used as a basis for determining the compositions of the simulated complex membranes [4]. Simulations of 13-MpPPC and 14-MpPPC provided baseline properties of pure iso- and anteiso-branched bilayers, while simulations of DPhPC enabled insight into the effect of the extent of branching on membrane properties. To this end, the surface area (SA) per lipid, electron density profiles (EDPs), area elastic moduli, deuterium order parameters, reorientational correlation functions and relaxation times were obtained for the bilayers described and are presented in this study.

2. Methods

Coordinates for pure lipid bilayers of 13-MpPPC, 14-MpPPC, and DPhPC were generated by modifying dipalmitoylphosphatidylcholine (DPPC) membrane coordinates generated from CHARMM-GUI Membrane Builder [18] and regenerating them using the appropriate topology. The DPhPC topology from Wataru Shinoda was modified to incorporate partial atomic charge changes in the PC head group for the C36 force field, and provided a basis for the atomic charges for the branches in the 13-MpPPC and 14-MpPPC topologies (standard values used for CHARMM alkanes). The generation and simulation of all three models allowed insight into the effects of branch position and the extent of branching on membrane properties. Each model consisted of 72 lipids and other details are in Table 1a.

The EB and RB membranes were designed to match the head group and lipid chain compositions determined from experimental methods [4]. To closely match the experimental compositions, a number of lipid types were synthesized by combining the appropriate head group and lipid chains. Table 1b shows the number of each lipid type used in the simulation models, while Tables 2a and b show the head group and lipid chain composition (% mol), respectively, of both the experimental and simulation models. The main discrepancy between the compositions of the experimental and simulation models is the amounts of 16:0 and 18:0 in RB. This was due to the use of POPE (18:1/16:0) instead of SOPE (18:1/18:0). The EB and RB membranes consisted of 250 lipids each.

All models were constructed using the membrane-only generation option in the Membrane Builder in CHARMM-GUI. Although a number of the lipid types, such as 13-MpPPC and 14-MpPPC, were not available, similar lipids (e.g. DPPC instead of 13-MpPPC) were used as a substitute in CHARMM-GUI and then modified to generate the coordinate sets for the desired lipids. A hydration of approximately 30 waters per lipid was used. The topologies for other newly created

Table 1a
Experimental setup of the lipid bilayers. Two independent simulation trajectories were used for each membrane.

Model	13-MpPPC	14-MpPPC	DPhPC	DPhPC	EB	RB
Temperature (K)	323.00	323.00	298.00	323.00	310.15	310.15
Number of lipids	72	72	72	72	250	250
Number of waters	2213	2213	2213	2213	7554	7494
Length (ns)	85/55	70/40	55/55	70/40	60/60	60/60
PME grid size	50×50×64	50×50×72	60×60×60	60×60×60	80×80×90	80×80×90

lipids, such as STPC, were based on combinations of existing head group and lipid chain topologies.

Once the membrane models were constructed, each was minimized in CHARMM [19] and then simulated using NAMD [20] with the all-atom parameter set of optimized lipid parameters (C36) [17] and the modified TIP3P water model [21]. The Steepest Descent algorithm (1000 steps) and the Adopted Basis Newton–Raphson algorithm (2000 steps) were used to minimize energies for high-energy contacts. This was followed by a 10-ns equilibration period. The exception is the second run of DPhPC at 298 K, which required a 43-ns equilibration period as indicated by the SA per lipid. The various production run times of the simulations are listed in Table 1a and totaled 0.470 μs.

MD trajectories of each system were generated using NAMD and two final snapshots are shown in Fig. 1. Two different simulations for each membrane model using a unique velocity seeding were run. 13-MpPPC and 14-MpPPC were simulated at 323 K to allow comparison to DPPC; DPhPC was simulated at both 298 K and 323 K for comparison to experimental data. The EB and RB membranes were simulated at 310.15 K to replicate physiological conditions. Langevin dynamics was used to maintain constant temperatures for each system, while the Langevin-piston algorithm was used to maintain constant pressure at 1 bar. A tetragonal unit cell was used to maintain an equal dimension between *X* and *Y* (in the plane of the membrane) while *Z* varied independently in the *NPT* (constant number of molecules, pressure, and temperature) ensemble. The van der Waals interactions were smoothly switched off at 8–10 Å by a potential switching function. This cutoff length is slightly smaller than what was used in the C36 force field development [17] but has a minor influence on the average area. Long-range electrostatic interactions were calculated using the particle-mesh Ewald (PME) method [22] with an interpolation order of 4, a direct space tolerance of 10^{-6}, and grid sizes that can be found in Table 1a. All bond lengths involving hydrogen atoms were fixed using the RATTLE algorithm [23]. A 2-fs time step was used, and coordinates were saved every ps for analysis.

Once the simulations were completed, the trajectories were analyzed to compare certain properties between the membranes. The overall SA per lipid, deuterium order parameters, and density profiles of all membranes were calculated. The deuterium order parameters are calculated via the following equation

$$|S_{CD}| = \left(\frac{1}{2}\right)\left(3\cos^2\theta - 1\right) \quad (1)$$

where θ is the average angle of a C-H vector with respect to the bilayer normal. Deuterium order parameters are typically reported as absolute values and this is assumed in our abbreviation (S_{CD}). The average SA of individual lipid components was also calculated for EB and RB using Voronoi tessellation[24,25]. The reorientational correlation functions (C_2) of 14-MpPPC (run 1), DPhPC at 323 K (run #1), and 14-MpPPC in the EB and RB membranes were also calculated and used to determine C21–C31 vector (μ) relaxation times (see Fig. 1 for atom labels) based on the following equation

$$C_2(t) = \langle P_2(\mu(0)\cdot\mu(t))\rangle \quad (2)$$

where P_2 is the second Legendre polynomial, $\frac{1}{2}\left(3x^2-1\right)$. Finally, the area elastic moduli of all membranes were calculated. The K_A of a bilayer is based on the area of the membrane system ($<A>$) and area fluctuations ($<\delta A^2>$), and is calculated via

$$K_A = k_B T <A> / <\delta A^2> \quad (3)$$

where k_B is Boltzmann's constant.

3. Results

The simulations were analyzed to investigate the effects of branching on various structural and dynamical properties. The SAs per lipid, EDPs, area elastic moduli, deuterium order parameters, reorientational correlation functions and relaxation times are presented herein.

3.1. Surface Areas per Lipid

The average SA is a well-known property of many lipid bilayers and is typically used to assess the accuracy of simulations. 13-MpPPC had a statistically higher average SA than 14-MpPPC (P-value<0.01) (Table 3). The average SA of 13-MpPPC and 14-MpPPC were quite close to the experimental SA of DPPC at 323 K (63 ± 1.0 Å^2) [26] and that calculated from a previous C36 simulation (Table 3). While 14-MpPPC had an SA per lipid statistically equivalent to that of DPPC simulated using the C36 force field with CHARMM and standard cutoffs, 13-MpPPC had a greater SA per lipid (Table 3) [17].

While the single-branched lipids had SAs per lipid quite close to that of DPPC, DPhPC dramatically increased SA per lipid relative to DPPC (Table 3). As expected, DPhPC exhibited a higher average SA at 323 K than at 298 K, increasing about 3–4 Å^2 with the temperature

Table 1b
Total number of lipids in the EB and RB membranes.

Model	13-MpPPC	14-MpPPC	DMPE	DOPE	DOPG	SLPC	PPPE	DSPE	DLPE	POPE	Chol
EB	8	42	8	46	8	22	26	6	0	0	84
RB	14	68	16	10	12	0	22	0	12	32	64

*13-MpPPC = 1-13-methylpentadecanoyl-2-palmitoyl-phosphatidylcholine (16:0/15:0BA).
*14-MpPPC = 1-14-methylpentadecanoyl-2-palmitoyl-phosphatidylcholine (16:0/15:0BI).
*DMPE = dimyristoylphosphatidylethanolamine (14:0/14:0).
*DOPE = dioleoylphosphatidylethanolamine (18:1/18:1).
*DOPG = dioleoylphosphatidylglycerol (18:1/18:1).
*SLPC = 1-stearoyl-2-lineoleoylphosphatidylcholine (18:0/18:2).
*PPPE = 1-palmitoyl-2-palmitoleoylphosphatidylethanolamine (16:0/16:1).
*DSPE = distearoylphosphatidylethanolamine (18:0/18:0).
*DTPE = dilineoleoylphosphatidylethanolamine (18:2/18:2).
*POPE = 1-palmitoyl-2-oleoylphosphatidylethanolamine (16:0/18:1).
*Chol = cholesterol.

Table 2a
Percent compositions of head groups in the EB and RB membranes. Experimental compositions were estimated from figures in the reference [4].

Model	PC	PE	PG	Chol
EB exp	27.5%	35.1%	3.3%	34.0%
EB sim	28.8%	34.4%	3.2%	33.6%
RB exp	32.5%	37.2%	4.6%	25.7%
RB sim	32.8%	36.8%	4.8%	25.6%

exp = experiment and sim = simulation.

Table 2b
Percent compositions of the phospholipid chains in the EB and RB membranes. Experimental compositions were estimated from figures in the reference [4].

Model	14:0	15:0BA	15:0BI	16:0	16:1	18:0	18:1	18:2
EB exp	5.2%	2.6%	13.1%	22.2%	7.8%	9.8%	32.7%	6.5%
EB sim	4.8%	2.4%	12.7%	22.9%	7.8%	10.2%	32.5%	6.6%
RB exp	8.2%	3.5%	17.6%	25.9%	5.3%	8.2%	25.9%	5.3%
RB sim	7.9%	3.5%	16.8%	33.7%	5.4%	0%	26.7%	5.9%

change. Moreover, the SA per lipid of DPhPC matched well with experiment and previous simulations. Wu et al. [8] determined the SA of DPhPC at 298 K to be 76 Å^2. More recent work by Tristram-Nagle et al. [6] determined the SA of DPhPC at 303.15 K to be 80.5 ± 1.5 Å^2. The average SA of the DPhPC production runs at 298 K was statistically equivalent to the experimental value at the same temperature.

The overall average SAs per lipid of the EB and RB membranes were also calculated (Table 3), as well as the average SA of each individual lipid component using Voronoi tessellation (Table S1). Overall, the average SAs of the EB and RB membranes were significantly lower than those of the pure membranes studied. This is not surprising given the amounts of cholesterol in the EB and RB membranes and cholesterol's well-known condensing effect [27,28]. It was expected that EB would have a lower average SA than RB, since EB had a higher cholesterol concentration. However, the effects of the phospholipids may have also had a role. Interestingly, the individual phospholipid areas were remarkably close, being only 1–3 Å^2 apart (Table S1).

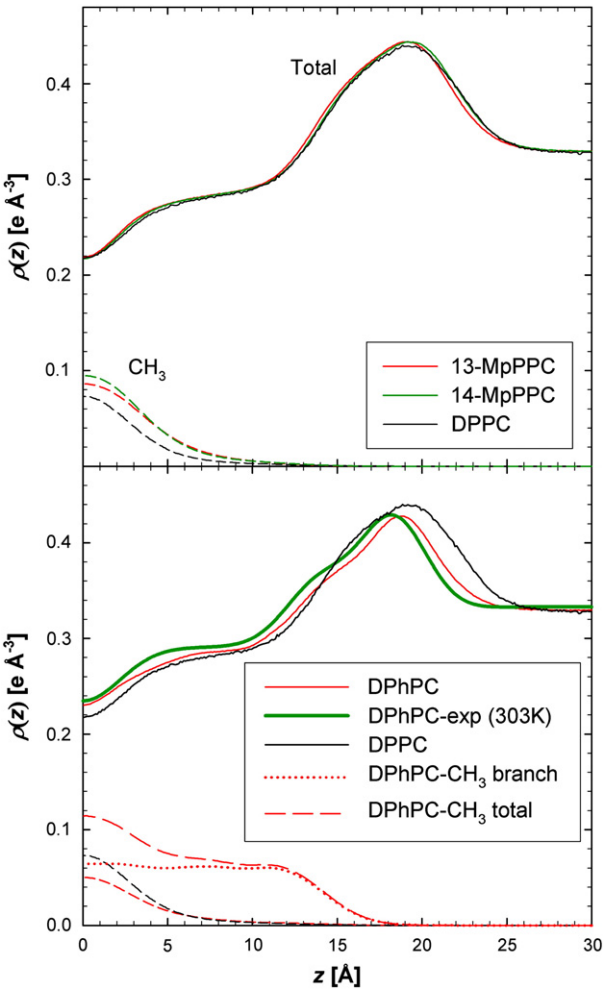

Fig. 2. (top) Average and symmetrized EDPs of 13-MpPPC, 14-MpPPC, and DPPC. (bottom) DPhPC and DPPC (323 K) with experimental DPhPC (303.15 K) [6]. DPPC was simulated using CHARMM and the C36 force field [17].

3.2. Electron density profiles

Although the SA of a lipid yields information about the membrane in the *XY*-plane, the EDP can reveal certain properties of the membrane along the *Z*-axis (membrane normal), such as membrane thickness, leaflet overlap, and the location of certain lipids and molecules. Typically, the EDP exhibits three regions: bulk water density ($|Z|>30$ Å), phospholipid head group ($|Z|\sim22$ Å), and a low-density trough ($Z=0$ Å).

The overall EDPs for 13-MpPPC and 14-MpPPC were very similar in shape and peak-to-peak distance to DPPC (Fig. 2, top). 13-MpPPC and 14-MpPPC had peak-to-peak distances of 37.9 Å and 38.4 Å, respectively, while DPPC had a peak-to-peak distance of 38.2 Å. A clear difference could be seen in the methyl component density between the single-branched lipids and DPPC. However, no discernible difference could be made in terms of the total density, which suggests that overall membrane properties were fairly independent of whether a single methyl branch was in place at the iso- or anteiso-position. While branching increased the methyl component density, this was a rather minor effect.

Interestingly, the methyl component density for the single-branched lipids was sharper and more distinct in the EB and RB membrane environments (Fig. 3). Furthermore, the single-branched lipids in the EB and RB membranes, when properly scaled, had a higher lipid density in the head group region than the pure form (Fig. 3). This may be partially explained by the higher peak-to-peak distance of the mixed membranes. The EB and RB membranes had peak-to-peak distances of 44.1 Å and 42.3 Å, respectively, while 13-MpPPC and 14-MpPPC had peak-to-peak distances of 37.9 Å and 38.4 Å, respectively.

The many methyl branches in DPhPC also have interesting effects on EDPs. DPhPC exhibited EDPs with a unique bump at approximately ± 15 Å in the *Z* direction (Fig. 2, bottom). Furthermore, the methylene component density in DPhPC was lower than in the single-branched lipids and DPPC by approximately 0.10 e Å^{-3}. Not surprisingly, DPhPC also had a higher methyl density than DPPC (Fig. 2, bottom) because of

Table 3
Average surface area (SA) per lipid of the lipid bilayer models. The two runs for each model were averaged to give the final value and standard error. The value for DPPC was taken from the reference [17].

Model	DPPC	13-MpPPC	14-MpPPC	DPhPC (298 K)	DPhPC (323 K)	EB	RB
Average SA (Å^2/lipid)	62.9 ± 0.3	63.8 ± 0.2	62.9 ± 0.2	76.1 ± 0.1	80.5 ± 0.1	47.14 ± 0.06	49.45 ± 0.06

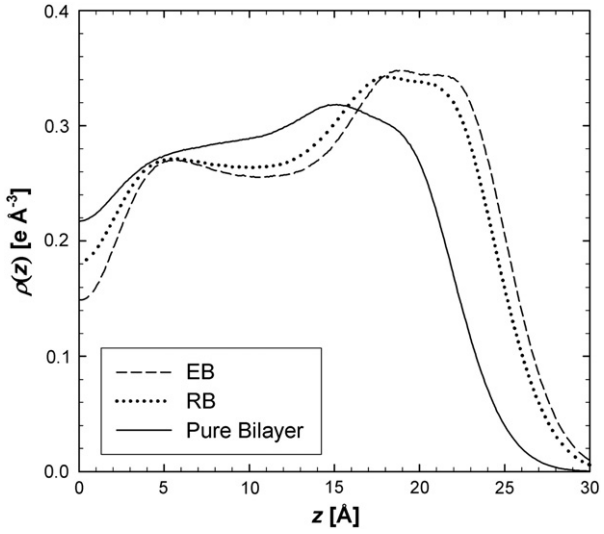

Fig. 3. Average EDPs of pure 14-MpPPC and in EB and RB (scaled to 250 lipids and independent of the EB and RB SA per lipid). Only the lipid component is shown (water is not included).

the methyl branches. DPPC did have a higher terminal methyl component density with 0.073 e $Å^{-3}$ at the bilayer center versus 0.050 e $Å^{-3}$ for DPhPC, though this may be due to displacement of the terminal methyl groups by the other methyl branches in DPhPC (Fig. 2, bottom).

Recently published data by Tristram-Nagle et al. [6] provided an experimental basis for comparison (Fig. 2, bottom). Although the experimental density was measured at 303.15 K, the density compares fairly well with our results at 323 K, as the shapes of the profiles were similar (Fig. 2, bottom). The experimental peak-to-peak distance was slightly smaller than what was determined from simulation; at 303.15 K, the peak-to-peak distance was 36.4 Å, while the distance calculated at 323 K was 37.6 Å. However, the average peak density measured at 303.15 K was 0.429 e $Å^{-3}$ and compared well with the average peak density of the 323 K simulation, which was 0.428 e $Å^{-3}$. The density at the low-density trough was slightly higher for experiment compared to the MD simulations.

3.3. Area elastic moduli

The area elastic modulus of a bilayer provides a measure of the membrane's stiffness, with a higher value indicating a stiffer membrane. For each system, the average and standard error were calculated and are listed in Table 4. The K_A of various bilayers has been determined experimentally by a variety of methods, including micropipette aspiration [29–40], deuterium NMR spectroscopy [41,42], and x-ray diffraction [42–48]. Rawicz et al. [40] found that K_A for lipids ranging in chain length from 13 carbons to 22 carbons and with varying levels of saturation, ranged from 229 ± 12 dyn/cm to 265 ± 18 dyn/cm. Although the K_A for DPhPC is not available experimentally, it was previously determined via simulation using the CHARMM27 lipid force field to be 670 dyn/cm at 298 K [15]. The K_A of the bilayer in this study are hence comparable to what has been determined experimentally and through simulation.

The area elastic moduli of the single-branched bilayers, 13-MpPPC and 14-MpPPC (Table 4), were determined to be slightly higher than the K_A of comparable lipids studied by Rawicz et al. [40]. Although statistically the K_A of 13-MpPPC was equivalent to the highest K_A determined by Rawicz et al. (DOPC), the K_A of 14-MpPPC was statistically higher than that of DOPC. Especially high were the values determined for DPhPC. Although lower than the value of 670 dyn/cm determined previously by simulation, the K_A of DPhPC calculated in this study were 605 ± 40 dyn/cm at 298 K and 522 ± 49 dyn/cm at 323 K, considerably higher than the area elastic moduli of the other pure bilayers in this study and the moduli determined in the literature.

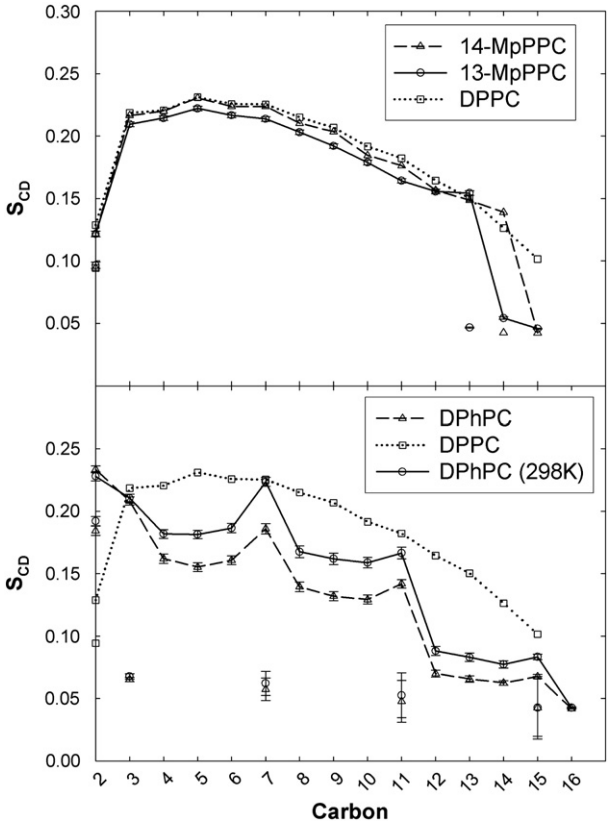

Fig. 4. Calculated aliphatic chain deuterium order parameters (S_{CD}) of the *sn-2* chain: (top) 13-MpPPC, 14-MpPPC, and DPPC [17] and (bottom) DPhPC (323 K), DPhPC (298 K) and DPPC [17]. Unless otherwise noted simulations are at 323 K.

3.4. Lipid aliphatic chain ordering

The deuterium order parameters (S_{CD}) for the aliphatic chains provide a quantitative measure of the chain order, where the higher the S_{CD}, the higher the chain order. Cholesterol is known to increase the order of surrounding aliphatic chains. The chain order is also known to be higher for saturated chains, and to decrease at unsaturated carbon positions.

The chain order of branched lipids was quite distinct from that of saturated or unsaturated lipid chains. 13-MpPPC, for instance, showed a sharp drop at the anteiso-position (Fig. 4, top). The carbons above the anteiso-position appeared to retain high order, undisturbed by the methyl branch down the chain. The order of these carbons was very similar to DPPC simulated with the C36 force field (Fig. 4, top); more specifically, the order of 14-MpPPC was comparable to that of DPPC, while the order of 13-MpPPC was slightly lower than that of both 14-MpPPC and DPPC. The order of the *sn-1* chain was also quite similar in

Table 4
Area elastic moduli of lipid bilayer models from Eq. (3). The two runs for each model were averaged to give the final value and standard error.

Model	13-MpPPC	14-MpPPC	DPhPC (298 K)	DPhPC (323 K)	EB	RB
K_A (dyn/cm)	274 ± 49	292 ± 9	605 ± 40	522 ± 49	583 ± 81	459 ± 7

magnitude and shape between the single-branched lipids and DPPC (Fig. S3). The presence of a methyl branch at a carbon position drastically decreased the order of both the methyl carbon and the main chain carbon to which the methyl branch was attached. Any carbons further down the chain consequently had a low order similar to that of the methyl branch and the carbon to which it was attached.

Overall, the S_{CD} for 13- and 14-MpPPC was highest in the EB membrane, followed by the RB membrane and then the pure form (Fig. 5). The S_{CD} of the EB membrane was comparable to that of POPE in a POPE/sphingomyelin/cholesterol mixture (33% cholesterol) measured at 303.15 K; although the shape differed slightly, 13-MpPPC in the EB membrane had a peak order of 0.3622, while POPE peaked at approximately 0.381 [49]. The magnitude of the order in the EB membrane was also comparable to that of DMPC in a DMPC/cholesterol mixture (30% cholesterol) at 298 K, which plateaued at 0.433, but had a shape more like that of 13-MpPPC in the EB membrane [50]. The order increased by approximately 75% from pure 13-/14-MpPPC to 13-/14-MpPPC in a mixed membrane. There was also a subtle difference in the shape of the S_{CD} plot between the pure lipid form of the single-branched lipids and the mixed form. While the S_{CD} began a steady decrease at the carbon 5 position for the pure lipid form of 13- and 14-MpPPC, the S_{CD} in the mixed bilayers continued to steadily increase until the carbon 7 position, at which point it began to slowly decline.

The order parameters of DPhPC exhibited very different behavior (Fig. 4, bottom). The S_{CD} of DPhPC as a function of carbon position had the same shape for both 298 and 323 K, with DPhPC at 298 K not surprisingly exhibiting a slightly higher order. The S_{CD} of DPhPC appeared to decrease in a step-wise fashion, with local maxima at main-chain carbons attached to methyl branches, i.e. carbon positions 3, 7, 11, and 15. The methyl branches themselves exhibited low order similar to that exhibited by the methyl branches in 13- and 14-MpPPC. There seemed to be a correlation between the S_{CD} of a methyl branch and its position on the chain, as the order of the methyl branches decreased sequentially from carbon position 3 down to carbon position 15. Each methyl branch seemed to signify a general decrease in the S_{CD}, or a "step" down. The overall order of DPhPC was lower than that of DPPC (Fig. 4, bottom), suggesting that additional methyl branches decrease the entire chain order in a membrane.

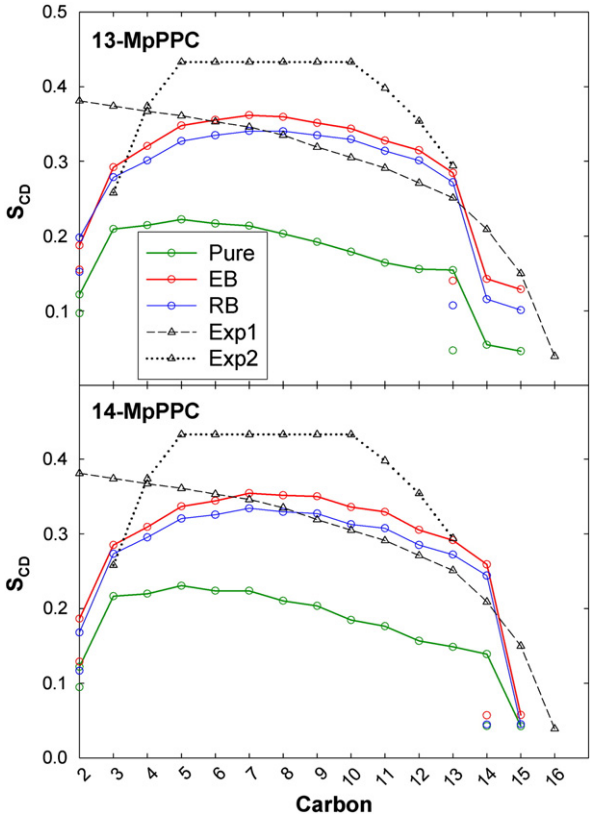

Fig. 5. Calculated aliphatic chain deuterium order parameters (S_{CD}) of the *sn-2* chain of pure 13-MpPPC (top) and 14-MpPPC (bottom) and in EB and RB. The experimental values for POPE and DMPC were measured from lipid membranes with the following compositions and temperatures respectively, POPE/spingomyelin/cholesterol (1:1:1) at 303.15 K [49] and DMPC/Chol (7:3) at 298 K [50].

3.5. Reorientational correlation functions and vector relaxation times

The reorientational correlation functions and vector relaxation times are related to lipid structure and the overall membrane environment, and can be estimated by NMR [51]. This study focuses on the rotational relaxation of the C21–C31 vector to represent rigid body movement of the acyl chains. The fitted amplitudes and decay times for the correlation functions are shown in Table 5. The value for α_0 was determined by calculating the square of the average S_{CD} value for the C21–C31 vector. This value was then fixed while the other parameters and relaxation times were fitted to the correlation function.

The fitted values indicate that as branching increases, all three relaxation times increase (Table 5 and Fig. 6). Again, the extra methyl branches were likely responsible. Adding one branch at the iso-position increased the slow relaxation time (τ_3), for instance, from 7.0 ns to 8.2 ns, which then increased to 20.0 ns for DPhPC. The extra branches appear to be slowing down the axial motions of the lipid, likely due to entangling between methyl branches of neighboring lipids. These motions are likely a combination of axial wobble and rotation [51] and motional models were not used to tease out these individual components.

We should note that we attempted to obtain relaxation times for 14-MpPPC in the EB and RB membranes. However, initial results indicate that the slow relaxation time was on the order of 50 ns or greater due to much slower decay times to reach a plateau, which would have required extension of the mixed membrane simulations to at least 100 ns for proper convergence. Hence, relaxation times for 14-MpPPC in the EB and RB membranes are not presented.

4. Discussion

We are the first to use the most recent CHARMM lipid force field, C36, to investigate branching in lipid bilayers. In general, based on our results, increased branching appears to increase the SA per lipid. The dramatic increase in SA per lipid from 62.9 ± 0.3 Å^2/lipid for DPPC to 80.5 ± 0.1 Å^2/lipid for DPhPC illustrates this clearly. Furthermore, our results agree well with previous studies. The average SA of DPhPC at 298 K was calculated to be 76.1 ± 0.1 Å^2/lipid, which is in very good agreement with the experimental value of 76 Å^2/lipid [8]. Previous simulations had determined average SAs of 77.7 Å^2/lipid [12] and 74.2 Å^2/lipid at 298 K [16] and 76.8 Å^2/lipid at 323 K [11]. More recently, Tristram-Nagle et al. [6] measured the SA of DPhPC at 303.15 K, determining it to be 80.5 ± 1.5 Å^2. Overall, our results are in good agreement with those of previous simulations and experiments.

Although no experimental order parameters have been published for DPhPC to date, our results are fairly comparable with previous

Table 5
Exponential fits to the reorientational correlation functions. Relaxation times are shown for the C21–C31 vector (Fig. 1). Parameters shown for DPPC are for the C27r lipid force field [50].

Model	α_1	α_2	α_3	α_0	τ_1 (ps)	τ_2 (ns)	τ_3 (ns)
DPPC	0.232	0.338	0.403	0.027	32.8	0.691	6.996
14-MpPPC	0.336	0.437	0.135	0.091	95.2	1.237	8.217
DPhPC	0.313	0.440	0.123	0.123	342.8	2.794	19.918

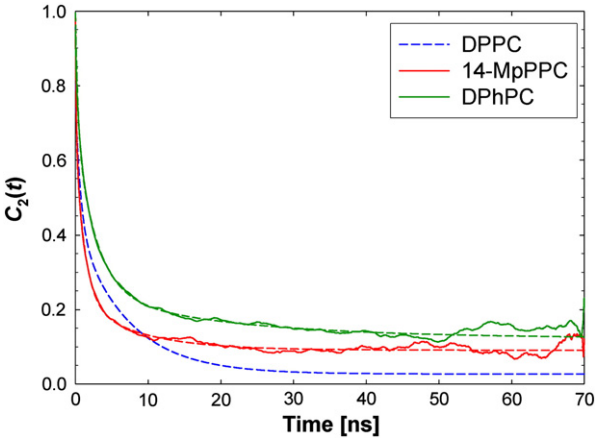

Fig. 6. Reorientational correlation functions of the C21–C31 vector for DPPC, 14-MpPPC, and DPhPC. The correlation function for DPPC was calculated using the C27r lipid force field [51]. Dashed lines indicate fits while solid lines indicate raw simulation data.

simulation results. The order parameters of DPhPC here agreed best with simulation results found by Shinoda et al. [11,16], who calculated DPhPC properties at 323 and 298 K. In these simulation studies, the CHARMM27 lipid force field was used and a step-wise decrease in S_{CD} going down the chain was similar to our results (Fig. 4, bottom) and lends further credence to the observation that methyl branches induce a decrease in chain order. In addition, local maxima in the profiles were shown at the C7, C11, and C15 positions at 298 K in both our study (Fig. 4, bottom) and Shinoda et al. [16]. The effect was not as pronounced at 323 K in the study by Shinoda et al. [11], though our order parameter profiles at 323 K also showed local maxima at those positions. The limited simulation time (1.5 ns) in the previous study by Shinoda et al. [11] suggests that their membranes may not have been as equilibrated as those in our study.

A key difference between our simulations and those done previously for DPhPC is the values for S_{CD} at the top of the aliphatic chain. Previous simulation studies show order parameter profiles with low order at the C2 carbon, which then rises with each succeeding carbon until finally reaching a plateau around the C4 or C5 carbon [11,16]. In our study, the C2 carbon has a relatively high order, 0.21, compared to 0.09 with C27 at 323 K. This is an important difference because while previous order parameter profiles showed a step-wise *increase* in order at the C3 carbon before subsequently decreasing in a step-wise fashion starting at the C7 carbon, our order parameter profiles showed a step-wise *decrease* starting at the C3 carbon. The cause for this change is the updated lipid force field. One of the key modifications to the CHARMM force field was to accurately obtain S_{CD} splitting at the C2 position as observed from experiment [17,52,53]. The order parameter for the C2 carbon on the *sn-1* chain does reach a maximum for the aliphatic carbons and there is an inequivalence to the hydrogens on the *sn-2* chain [17,52,53]. This occurs with the DPhPC simulations but the order of the *sn-2* chain remains high for the C2 position likely due to the presence of the neighboring methyl branch.

While deuterium order parameters for DPhPC decreased in a step-wise fashion, those for 13-MpPPC and 14-MpPPC were extremely similar to those for DPPC above the iso- and anteiso-positions. The C2 hydrogen splitting was similar in magnitude for all three lipid types, and the S_{CD} plots for all three had very similar shapes. 13-MpPPC had a slightly lower order in this region of the chain, suggesting that a branch at the anteiso-position rather than the iso-position causes slightly more chain disorder. At the anteiso- and iso-positions, both of the single-branched lipids exhibit a precipitous drop in order, marking the greatest difference between the single-branched lipids and DPPC in terms of order parameters.

Although the electron density profile of DPhPC has been measured at 298 and 303.15 K, we decided to compare our results with the more recent and rigorous experimental study of DPhPC at 303.15 K [6]. The experimental and simulation temperatures differ slightly, but our density profiles did exhibit the same shape as the experimental profile (Fig. 2). Furthermore, while the peak-to-peak distances at 298 K (38.6 Å) and 323 K (37.6 Å) were somewhat higher than the experimental value (36.4 Å), the magnitudes of the densities calculated at 323 K and measured at 303.15 K were comparable. The agreements in EDP shape and peak-to-peak distance between our results and previous experimental studies support the validity of the C36 parameters used in this study.

There was little difference in the EDPs between the single-branched lipids (13-MpPPC and 14-MpPPC) and DPPC. However, DPhPC showed a rougher EDP. This can be attributed to the methyl branches, which add extra density at those z positions but also repel other DPhPC molecules. From the EDPs, single-branched membranes appear to have structural properties similar to those of DPPC; however, membranes with multiples branches such as DPhPC are entirely different structurally. Further branching leads to further deviation from DPPC structure.

The area elastic moduli determined for this study show that branching tends to increase bilayer stiffness. The single-branched lipids had slightly higher area elastic moduli than more typical lipids studied (Table 4). DPhPC, however, had much higher elastic moduli (Table 4). Again, the methyl branches of the disordered chains may be entangling and interacting, which in turn may increase the stiffness. Since DPhPC has more methyl branches than 13-MpPPC or 14-MpPPC, DPhPC likely had higher stabilization energy due to these methyl branches, resulting in an increase in overall stiffness. Although the area elastic modulus of DPhPC was lower than in previous simulation studies [15], this decrease is consistent with an overall decrease using the new C36 force field parameters, a trend that is generally in better agreement with experiment [17].

Lastly, branching also significantly impacted the axial relaxation times probed by the C21–C31 vector. Fast, intermediate and slow relaxation times increased with increased branching (Table 5), indicating a clear trend. Again, we hypothesize that interactions between methyl branches of neighboring lipids are responsible. The increased number of methyl branches likely leads to increased entangling between lipids, which would physically slow down the rotational motions of the lipids.

The K_A of the mixed membranes were relatively high due to the high amount of cholesterol, which is consistent with experiment. Evans and Rawicz, for instance, found that K_A increased from 190 ± 10 dyn/cm for 1-stearoyl-2-oleoylphosphatidylcholine (SOPC) to 640 ± 32 dyn/cm for a SOPC:Chol bilayer (1:1 mol ratio) [29]. Tierney et al. [38] found that the area elastic modulus of a DPPC:Chol bilayer (9:1 mol ratio) increased from 407.6 ± 130.2 dyn/cm to 1281.2 ± 140.8 dyn/cm upon the addition of cholesterol (1:1 mol ratio). Therefore, the high elastic moduli of the mixed membranes relative to those of the pure bilayers were not surprising. The EB membrane had a cholesterol concentration 8% higher than that of the RB membrane, which helps account for the higher K_A for EB membranes compared to the RB membranes.

While it is unclear whether the single-branched lipids in the EB and RB membranes contribute to their high elastic moduli, this property may have potential biological implications. The high elastic moduli lead to greater membrane stiffness, which in turn may make it easier for EBs to penetrate host cells. This increased stiffness may also help EBs and RBs help maintain membrane integrity throughout the biphasic cycle, particular the cell lysing step. The higher cholesterol concentration in the EB relative to the RB and the resulting higher K_A also make sense given EB's role as a metabolically inactive body, as greater stiffness would make the EB less permeable to solutes.

5. Conclusions

In conclusion, we are the first to report MD simulations of the single-branched lipids 13-MpPPC and 14-MpPPC. We are also the first to study DPhPC using the recently developed C36 lipid force field, as well as the first to study complex, realistic membranes found in *Chlamydia trachomatis*. Our results show the effect of lipid chain branching on a number of important biophysical properties, including SA per lipid, deuterium order parameters, EDPs, area elastic moduli, and lipid axial relaxation times. Branching was found to increase bilayer SA, decrease chain order, increase area elastic moduli, and increase axial relaxation times. Branching also had a distinct effect on the shapes and peak-to-peak distances of the EDPs. Finally, our study of complex membranes found in the Chlamydia bacterium provided insight into the biophysical properties of such membranes. This will ultimately prove useful in studies of peptides from the major outer membrane porin protein, which holds promise as a potential vaccine candidate.

Acknowledgments

We are grateful to Dr. Wataru Shinoda for providing the topology of DPhPC and Drs. Stephanie Tristram-Nagle and John Nagle for providing us the experimental electron density profiles of DPhPC. This work was supported by institutional funding from the University of Maryland (J.B.K) and a Howard Hughes Medical Institute Undergraduate Research Fellowship (J.B.L).

Appendix A. Supplementary data

Supplementary data to this article can be found online at doi:10.1016/j.bbamem.2010.07.036.

References

[1] Y. Wang, E.A. Berg, X. Feng, L. Shen, T. Smith, C.E. Costello, Y.-X. Zhang, Identification of surface-exposed components of MOMP of *Chlamydia trachomatis* serovar F, Protein Sci. 15 (2006) 122–134.
[2] G. Sun, S. Pal, A.K. Sarcon, S. Kim, E. Sugawara, H. Nikaido, M.J. Cocco, E.M. Peterson, L.M. de la Maza, Structural and functional analyses of the major outer membrane protein of *Chlamydia trachomatis*, J. Bacteriol. 189 (2007) 6222–6235.
[3] G.M. Hatch, G. McClarty, Phospholipid composition of purified *Chlamydia trachomatis* mimics that of the eucaryotic host cell, Infect. Immun. 66 (1998) 3727–3735.
[4] J.L. Wylie, G.M. Hatch, G. McClarty, Host cell phospholipids are trafficked to and then modified by *Chlamydia trachomatis*, J. Bacteriol. 179 (1997) 7233–7242.
[5] T. Kaneda, Iso- and anteiso-fatty acids in bacteria: biosynthesis, function, and taxonomic significance, Microbiol. Mol. Biol. Rev. 55 (1991) 288–302.
[6] S. Tristram-Nagle, D.J. Kim, N. Akhunzada, N. Kucerka, J.C. Mathai, J. Katsaras, M. Zeidel, J.F. Nagle, Structure and water permeability of fully hydrated diphytanoylPC, Chem. Phys. Lipids 163 (2010) 630–637.
[7] T. Baba, H. Minamikawa, M. Hato, T. Handa, Hydration and molecular motions in synthetic phytanyl-chained glycolipid vesicle membranes, Biophys. J. 81 (2001) 3377–3386.
[8] Y. Wu, K. He, S.J. Ludtke, H.W. Huang, X-ray diffraction study of lipid bilayer membranes interacting with amphiphilic helical peptides: diphytanoyl phosphatidylcholine with alamethicin at low concentrations, Biophys. J. 68 (1995) 2361–2369.
[9] T. Husslein, D.M. Newns, P.C. Pattnaik, Q. Zhong, P.B. Moore, M.L. Klein, Constant pressure and temperature molecular-dynamics simulation of the hydrated diphytanolphosphatidylcholine lipid bilayer, J. Chem. Phys. 109 (1998) 2826–2832.
[10] T. Husslein, P.B. Moore, Q. Zhong, D.M. Newns, P.C. Pattnaik, M.L. Klein, Molecular dynamics simulation of a hydrated diphytanol phosphatidylcholine lipid bilayer containing an alpha-helical bundle of four transmembrane domains of the Influenza A virus M2 protein, Faraday Discuss. 111 (1998) 201–208.
[11] W. Shinoda, M. Mikami, T. Baba, H. Masakatsu, Molecular dynamics study on the effect of chain branching on the physical properties of lipid bilayers: structural stability, J. Phys. Chem. B 107 (2003) 14030–14035.
[12] K. Shinoda, W. Shinoda, T. Baba, M. Mikami, Comparative molecular dynamics study of ether- and ester-linked phospholipid bilayers, J. Chem. Phys. 121 (2004) 9648–9654.
[13] W. Shinoda, M. Mikami, T. Baba, M. Hato, Dynamics of a highly branched lipid bilayer: a molecular dynamics study, Chem. Phys. Lett. 390 (2004) 35–40.
[14] W. Shinoda, M. Mikami, T. Baba, M. Hato, Molecular dynamics study on the effects of chain branching on the physical properties of lipid bilayers: 2. Permeability, J. Phys. Chem. B 108 (2004) 9346–9356.
[15] W. Shinoda, K. Shinoda, T. Baba, M. Mikami, Molecular dynamics study of bipolar tetraether lipid membranes, Biophys. J. 89 (2005) 3195–3202.
[16] K. Shinoda, W. Shinoda, M. Mikami, Molecular dynamics simulation of an archaeal lipid bilayer with sodium chloride, Phys. Chem. Chem. Phys. 9 (2007) 643–650.
[17] J.B. Klauda, R.M. Venable, J.A. Freites, J.W. O'Connor, C. Mondragon-Ramirez, I. Vorobyov, D.J. Tobias, A.D. MacKerell, R.W. Pastor, Update of the CHARMM all-atom additive force field for lipids: validation on six lipid types, J. Phys. Chem. B 114 (2010) 7830–7843.
[18] S. Jo, T. Kim, V.G. Iyer, W. Im, CHARMM-GUI: a web-based graphical user interface for CHARMM, J. Comput. Chem. 29 (2008) 1859–1865.
[19] B.R. Brooks, I.C.L. Brooks, J.A.D. Mackerell, L. Nilsson, R.J. Petrella, B. Roux, Y. Won, G. Archontis, C. Bartels, S. Boresch, A. Caflisch, L. Caves, Q. Cui, A.R. Dinner, M. Feig, S. Fischer, J. Gao, M. Hodoscek, W. Im, K. Kuczera, T. Lazaridis, J. Ma, V. Ovchinnikov, E. Paci, R.W. Pastor, C.B. Post, J.Z. Pu, M. Schaefer, B. Tidor, R.M. Venable, H.L. Woodcock, X. Wu, W. Yang, D.M. York, M. Karplus, CHARMM: the biomolecular simulation program, J. Comput. Chem. 30 (2009) 1545–1614.
[20] J.C. Phillips, R. Braun, W. Wang, J. Gumbart, E. Tajkhorshid, E. Villa, C. Chipot, R.D. Skeel, L. Kale, K. Schulten, Scalable molecular dynamics with NAMD, J. Comput. Chem. 26 (2005) 1781–1802.
[21] W.L. Jorgensen, J. Chandrasekhar, J.D. Madura, R.W. Impey, M.L. Klein, Comparison of simple potential functions for simulating liquid water, J. Chem. Phys. 79 (1983) 926–935.
[22] U. Essmann, L. Perera, M.L. Berkowitz, T. Darden, H. Lee, L.C. Pedersen, A smooth particle mesh Ewald method, J. Chem. Phys. 103 (1995) 8577–8593.
[23] H.C. Andersen, Rattle—a velocity version of the SHAKE algorithm for molecular-dynamics calculations, J. Comput. Phys. 52 (1983) 24–34.
[24] S.A. Pandit, S. Vasudevan, S.W. Chiu, R.J. Mashl, E. Jakobsson, H.L. Scott, Sphingomyelin-cholesterol domains in phospholipid membranes: atomistic simulation, Biophys. J. 87 (2004) 1092–1100.
[25] W. Shinoda, S. Okazaki, A Voronoi analysis of lipid area fluctuation in a bilayer, J. Chem. Phys. 109 (1998) 1517–1521.
[26] N. Kučerka, J.F. Nagle, J.N. Sachs, S.E. Feller, J. Pencer, A. Jackson, J. Katsaras, Lipid bilayer structure determined by the simultaneous analysis of neutron and x-ray scattering data, Biophys. J. 95 (2008) 2356–2367.
[27] W.-C. Hung, M.-T. Lee, F.-Y. Chen, H.W. Huang, The condensing effect of cholesterol in lipid bilayers, Biophys. J. 92 (2007) 3960–3967.
[28] T.J. McIntosh, Effect of cholesterol on structure of phosphatidylcholine bilayers, Biochim. Biophys. Acta 513 (1978) 43–58.
[29] E. Evans, W. Rawicz, Entropy-driven tension and bending elasticity in condensed-fluid membranes, Phys. Rev. Lett. 64 (1990) 2094–2097.
[30] N. Fa, L. Lins, P.J. Courtoy, Y. Dufrêne, P. Van Der Smissen, R. Brasseur, D. Tyteca, M.-P. Mingeot-Leclercq, Decrease of elastic moduli of DOPC bilayers induced by a macrolide antibiotic, azithromycin, Biochim. Biophys. Acta 1768 (2007) 1830–1838.
[31] J. Henriksen, A.C. Rowat, E. Brief, Y.W. Hsueh, J.L. Thewalt, M.J. Zuckermann, J.H. Ipsen, Universal behavior of membranes with sterols, Biophys. J. 90 (2006) 1639–1649.
[32] H.V. Ly, D.E. Block, M.L. Longo, Interfacial tension effect of ethanol on lipid bilayer rigidity, stability, and area/molecule: a micropipet aspiration approach, Langmuir 18 (2002) 8988–8995.
[33] H.V. Ly, M.L. Longo, The influence of short-chain alcohols on interfacial tension, mechanical properties, area/molecule, and permeability of fluid lipid bilayers, Biophys. J. 87 (2004) 1013–1033.
[34] D. Needham, E. Evans, Structure and mechanical properties of giant lipid (DMPC) vesicle bilayers from 20 °C below to 10 °C above the liquid crystal–crystalline phase transition at 24 °C, Biochemistry 27 (1988) 8261–8269.
[35] D. Needham, T.J. McIntosh, E. Evans, Thermomechanical and transition properties of dimyristoylphosphatidylcholine/cholesterol bilayers, Biochemistry 27 (1988) 4668–4673.
[36] D. Needham, R.M. Hochmuth, Electro-mechanical permeabilization of lipid vesicles: role of membrane tension and compressibility, Biophys. J. 55 (1989) 1001–1009.
[37] D. Needham, R.S. Nunn, Elastic deformation and failure of lipid bilayer membranes containing cholesterol, Biophys. J. 58 (1990) 997–1009.
[38] K.J. Tierney, D.E. Block, M.L. Longo, Elasticity and phase behavior of DPPC membrane modulated by cholesterol, ergosterol, and ethanol, Biophys. J. 89 (2005) 2481–2493.
[39] Y. Zhou, R.M. Raphael, Effect of salicylate on the elasticity, bending stiffness, and strength of SOPC membranes, Biophys. J. 89 (2005) 1789–1801.
[40] W. Rawicz, K.C. Olbrich, T. McIntosh, D. Needham, E. Evans, Effect of Chain Length and Unsaturation on Elasticity of Lipid Bilayers, 79 (2000) 328-339.
[41] M.F. Brown, R.L. Thurmond, S.W. Dodd, O. Dörte, K. Beyer, Elastic deformation of membrane bilayers probed by deuterium NMR relaxation, J. Am. Chem. Soc. 124 (2002) 8471–8484.
[42] B.W. Koenig, H.H. Strey, K. Gawrisch, Membrane lateral compressibility determined by NMR and X-Ray diffraction: effect of acyl chain polyunsaturation, Biophys. J. 73 (1997) 1954–1966.
[43] D. Allende, S.A. Simon, T.J. McIntosh, Melittin-induced bilayer leakage depends on lipid material properties: evidence for toroidal pores, Biophys. J. 88 (2005) 1828–1837.
[44] H. Binder, K. Gawrisch, Effect of unsaturated lipid chains on dimensions, molecular order and hydration of membranes, J. Phys. Chem. B 105 (2001) 12378–12390.
[45] J. Pan, S. Tristram-Nagle, N. Kučerka, J.F. Nagle, Temperature dependence of structure, bending rigidity, and bilayer interactions of dioleoylphosphatidylcholine bilayers, Biophys. J. 94 (2008) 117–124.
[46] J. Pan, S. Tristram-Nagle, J.F. Nagle, Effect of cholesterol on structural and mechanical properties of membranes depends on lipid chain saturation, Phys. Rev. E 80 (2009).
[47] S. Tristram-Nagle, Y.F. Liu, J. Legleiter, J.F. Nagle, Structure of gel phase DMPC determined by X-ray diffraction, Biophys. J. 83 (2002) 3324–3335.

[48] S. Tristram-Nagle, H.I. Petrarche, J.F. Nagle, Structure and interactions of fully hydrated dioleoylphosphatidylcholine bilayers, Biophys. J. 75 (1998) 917–925.
[49] S.R. Shaikh, M.R. Brzustowicz, N. Gustafson, W. Stillwell, S.R. Wassall, Monounsaturated PE does not phase-separate from the lipid raft molecules sphingomyelin and cholesterol: role for polyunsaturation? Biochemistry 41 (2002) 10593–10602.
[50] J.-P. Douliez, A. Leonard, E.J. Dufourc, Restatement of order parameters in biomembranes: calculation of C-C bond order parameters from C-D quadrupolar splittings, Biophys. J. 68 (1995) 1727–1739.
[51] J.B. Klauda, M.F. Roberts, A.G. Redfield, B.R. Brooks, R.W. Pastor, Rotation of lipids in membranes: molecular dynamics simulation, ^{31}P Spin-lattice relaxation, and rigid-body dynamics, Biophys. J. 94 (2008) 3074–3083.
[52] A. Seelig, J. Seelig, The dynamic structure of fatty acyl chains in a phospholipid bilayer measured by deuterium magnetic resonance, Biochemistry 13 (1974) 4839–4845.
[53] A. Seelig, J. Seelig, Bilayers of dipalmitoyl-3-sn-phosphatidylcholine—conformational differences between fatty acyl chains, Biochim. Biophys. Acta 406 (1975) 1–5.